CrystEngComm

Accepted Manuscript

Facile preparation of Chevreul's salt (Cu$_2$SO$_3$·CuSO$_3$·2H$_2$O) mesocrystalline microspheres and its high photocatalytic activity†

Mingyun Guan,* [a] Yan Jian,[a] Jianhua Sun,[a] Tongming Shang,[a] Qi Liu,[b] and Zheng Xu* [c]

Cu$_2$SO$_3$·CuSO$_3$·2H$_2$O mesocrystalline microspheres were successfully prepared by a facile method for the first time. Section image of the products displayed that microspheres included a peanut-like core consisting of packed particles and a shell composed of particles in oriented attachment fashion. Acetic acid played a key role in the formation of Cu$_2$SO$_3$·CuSO$_3$·2H$_2$O mesocrystalline microspheres. The possible formation mechanism was proposed. The mesocrystalline microspheres presented excellent photocatalytic performance for decomposition of organic compounds under the UV light irradiation such as RhB, acid fuchsin, thymol blue, MB (being completely decomposed) and MO (94%). Moreover, high photocatalytic activity of mesocrystalline microsphere was retained after cycling several times. They may have promising application for the treatment of contaminated water.

1. Introduction

Removal of organic pollution from the waste water is severe issue in modern society both daily life and industrial environments owing to high toxicity and tremendous kinds of ogranic pollutions. Due to low concentration, organic pollutions are difficult to be completely removed from the waste water using tranditional techniques such as adsorption, ultrafiltration, and coagulation, *etc*. Photocatalysis technique captures more attentions from researchers due to being "green", low-cost and removing the organic pollutants rapidly since TiO$_2$ is found to be an excellent photocatalyst for decomposing many organic compounds [1, 2]. In order to obtain robust photocatalysts with high photocatalytic activity, on the one hand, people search for a new class of photocatalysts; on the other hand, improve properties of the existed photocatalysts by changing their morphologies, sizes, phase structure, specific surface area, or doping different ions, *etc* [3-6].

In recent years, nano-scale photocatalysts exhibited excellent photocatalytic performances for the treatment of waste water due to small size, high specific surface area, and immense high

[a] *Jiangsu Key Laboratory of Precious Metals Chemistry, School of Chemistry and Environmental Engineering, Jiangsu University of Technology, Changzhou, 213001, P. R. China, E-mail: guanmy@jsut.edu.cn*
[b] *School of Petrochemical Engineering, Changzhou University, Changzhou 213164, P. R. China.*
[c] *State Key Laboratory of Coordination Chemistry, School of Chemistry and Chemical Engineering, Nanjing University, Nanjing, 210093, P. R. China, E-mail: zhengxu@nju.edu.cn, Fax: +86-25-83314502.*
† Electronic supplementary information (ESI) available: Temporal UV-vis absorption spectral changes for the dyes solution over Cu$_2$SO$_3$·CuSO$_3$·2H$_2$O mesocrystalline microsphere as a function of UV irradiation time. Detailed synthesis procedure Of Cu$_2$SO$_3$·CuSO$_3$·2H$_2$O irregular microparticles. Pore-size distribution isotherms of Cu$_2$SO$_3$·CuSO$_3$·2H$_2$O mesocrystalline microspheres.

activity [7-9]. However, there are several problems in the nanocatalytic area to be resolved before use. For example, the activities of catalysts decrease owing to aggregation of nanoparticles in the reaction medium. Additionally, due to the small sizes, nanoparticles are difficult to be handled and may produce secondary pollution which arouses the public concerns about the safety of nanomaterials [10-12]. It is urgent to find new class of materials which not only has excellent catalytic performance and also has large size. Mesocrystalline materials may be a promising candidate. Mesocrystal is a novel class of solid material which is constructed by small particles instead of atom/molecule as building blocks in oriented-attachment fashion[13-16]. Remarkable characters of mesocrystalline materials are high porosity and own properties passing from small build units. High porosity is benefic for diffusion of dyes solution into the interior of catalysts. Small-size build units have more active sites and good crystalline which is advantageous of electrons and holes transfer. Additionally, relatively larger sizes are easy to be handled and relieve public concerns about secondary pollution [17]. Very recent, there were a few reports about catalytic performance of mesocrystals [13, 14, 18-23].

Since the first mixed-valence sulfites complex, $Cu_2SO_3 \cdot CuSO_3 \cdot 2H_2O$, was synthesized by M. Chevreul in 1812 [24], study on this type of compound was intensified till its crystalline structure was determined by Kiekegaard and Nyberg in the mid-1960s [25]. Conklin and Hoffmann (1988) investigated the structure, thermodynamics and kinetics properties of metal ion-sulfur (IV) chemistry [26, 27]. Tang and coauthor prepared durian-like structure of $Cu_2SO_3 \cdot CuSO_3 \cdot 2H_2O$ and found it was not suitable for lithium ion battery electrode material [28]. In addition, their spectroscopic, magnetic and thermal properties were characterized [29-33]. But as a sum of the two separate metal ions, reports on the mixed-valence sulfites complex were still less. There were also no reports on controlled synthesis of morphologies and sizes, and related chemical properties. We noticed the strong adsorption peak at 400-500 nm appeared in UV-vis diffuse reflectance spectra of $Cu_2SO_3 \cdot MSO_3 \cdot 2H_2O$ (Cu, Fe, Mn and Cd), and wanted to know whether it could be used as photocatalyst to degrade organic contaminants. Herein by adding acetic acid into Na_2SO_3 and $Cu(CH_3COO)_2$ mixture solution, $Cu_2SO_3 \cdot Cu_SO_3 \cdot 2H_2O$ mesocrystalline microspheres were synthesized at the ambient temperature in a few minutes. The method was facile and feasible. The mesocrystalline microspheres consisted of small particles and owned high porosity. It could efficiently degrade the various kinds of organic dyes under the ultraviolet light irradiation. High

2

photocatalytic activities were still retained after cycling many times. The possible formation and catalytic mechanisms were proposed. It is the fist report on synthesis of uniform morphologies and chemical properties about $Cu_2SO_3 \cdot MSO_3 \cdot 2H_2O$ and it would again rekindle the interest of researchers on this type of compound.

2. Experimental Section

2.1 Materials

All chemicals used in this study were of analytical grade and were used without further purification. Cupric acetate ($Cu(CH_3COO)_2 \cdot H_2O$, $CuAc_2$), sodium sulfite anhydrous (Na_2SO_3), acetic acid (CH_3COOH, HAc, >99.5%), terephthalic acid (TA), NaOH, and sulphuric acid (H_2SO_4) were purchased from Shanghai Guoyao Chemical Reagent Company. P25 (TiO_2) was purchased from Degussa Corporation (particle size of 21 nm, BET area of 50 $m^2 \cdot g^{-1}$).

2.2 Synthesis of $Cu_2SO_3 \cdot CuSO_3 \cdot 2H_2O$ mesocrystalline microspheres

20 mL Na_2SO_3 (7.6 mmol$\cdot L^{-1}$) aqueous solution was added into 20 mL $CuAc_2$ (4.67 mmol $\cdot L^{-1}$) aqueous solution in a beaker under magnetic stirring at the ambient temperature. The slurry immediately formed. After stirring for 15 min, 5 mL HAc (>99.5%) solution was added into the mixed solution. The slurry rapidly became transparent and then brick red materials produced in the solution. Stopping stir, the brick red precipitates at the bottom of the beaker were collected after 15 min, washed with distilled water, and then dried in a vacuum oven at 80℃.

2.3 Synthesis of Cu_2O hollow spheres

20 mL of Na_2SO_3 aqueous solution (7.6 mmol$\cdot L^{-1}$) was added into 20 mL of $Cu(Ac)_2$ aqueous solution (4.67 mmol$\cdot L^{-1}$) in 100 mL beaker under stirring for 5 min. The beaker was sealed and transferred into oven and maintained at 95℃ for 4 h. The red precipitate at the bottom of beaker were collected, washed with distilled water, and then dried in a vacuum oven at 80℃.

2.4 Characterization

3

X-ray powder diffraction (XRD) was carried out on diffractometer with Cu-Kα radiation (λ = 1.5418 Å) in the range of 2θ =10–80°. Scanning electron microscopy (SEM) and field emission SEM (FESEM) images were taken on a Hitachi S3400N scanning electron microscope and S4800 field emission scanning electron microscope respectively. Transmission electron microscopy (TEM), high-resolution TEM (HRTEM) images and fast Fourier-transform pattern were recorded on a Philips Tecnai 20 electron microscope, using an accelerating voltage of 200 kV. Brunauer-Emmett-Teller (BET) specific surface area of the powders was analyzed by nitrogen adsorption in a Micromeritics ASAP 2020 nitrogen adsorption apparatus (USA). All the as-prepared samples were degassed at 150℃ for 4 h prior to nitrogen adsorption measurements. UV-vis diffuse reflectance of the sample was measured using Shimadzu SolidSpec-3700 spectrophotometer (Japan). Photoluminescence spectra were recorded on a Cary Eclipse photoluminescence spectrometer at room temperature (Varian, USA).

2.5 Detection of hydroxyl radicals (·OH)

Typically, 0.1 g of the as-prepared product was dispersed in a 20 mL of TA aqueous solution (1.5 mmol·L^{-1}) with a concentration of 6 mmol·L^{-1} NaOH. The solution was stirred for 15 min to reach homogeneity at room temperature. After that, the solution was irradiated with a 500 W high-voltage mercury lamp. After irradiation every 15 min, 4 mL of the solution was sampled and separated by centrifugation to remove the photocatalyst. The fluorescence intensity at 426 nm was monitored on a Cary Eclipse fluorescence spectrophotometer excited by 315 nm light.

2.6 Photocatalytic activity test

The photocatalytic activity of $Cu_2SO_3 \cdot CuSO_3 \cdot 2H_2O$ mesocrystalline microspheres was evaluated by degrading aqueous solution containing different organic dyes such as rhodamine B (RhB), methyl blue (MB), methyl orange (MO), thymol blue, or acid fuchsin under UV light irradiation. The detailed measuring procedure was as followed using RhB as representative sample. In the typical experiment, 0.03 g $Cu_2SO_3 \cdot CuSO_3 \cdot 2H_2O$ powder was added into 50 mL RhB aqueous solution (20 mg·L^{-1}) in a reactor at room temperature. Prior to irradiation, the solution was stirred for 15 min in dark to ensure the establishment of an adsorption–desorption equilibrium.

Then, the solution was exposed to 500 W high-voltage mercury lamp light irradiation under

magnetic stirring. At each given time interval, 4 mL suspension was sampled and centrifuged to

remove the $Cu_2SO_3 \cdot CuSO_3 \cdot 2H_2O$ powder. The concentration of RhB during the degradation was

monitored by using a Shimadzu UV3600 spectrophotometer. All of the measurements were carried

out at the room temperature. The photocatalytic activity of $Cu_2SO_3 \cdot CuSO_3 \cdot 2H_2O$ irregular

micro-particles and P25 were evaluated using the same way. Total organic carbon analyzer

(TOC-Vwp, Shimadzu) was employed for mineralization degree analysis of RhB solutions.

3. Results and Discussion
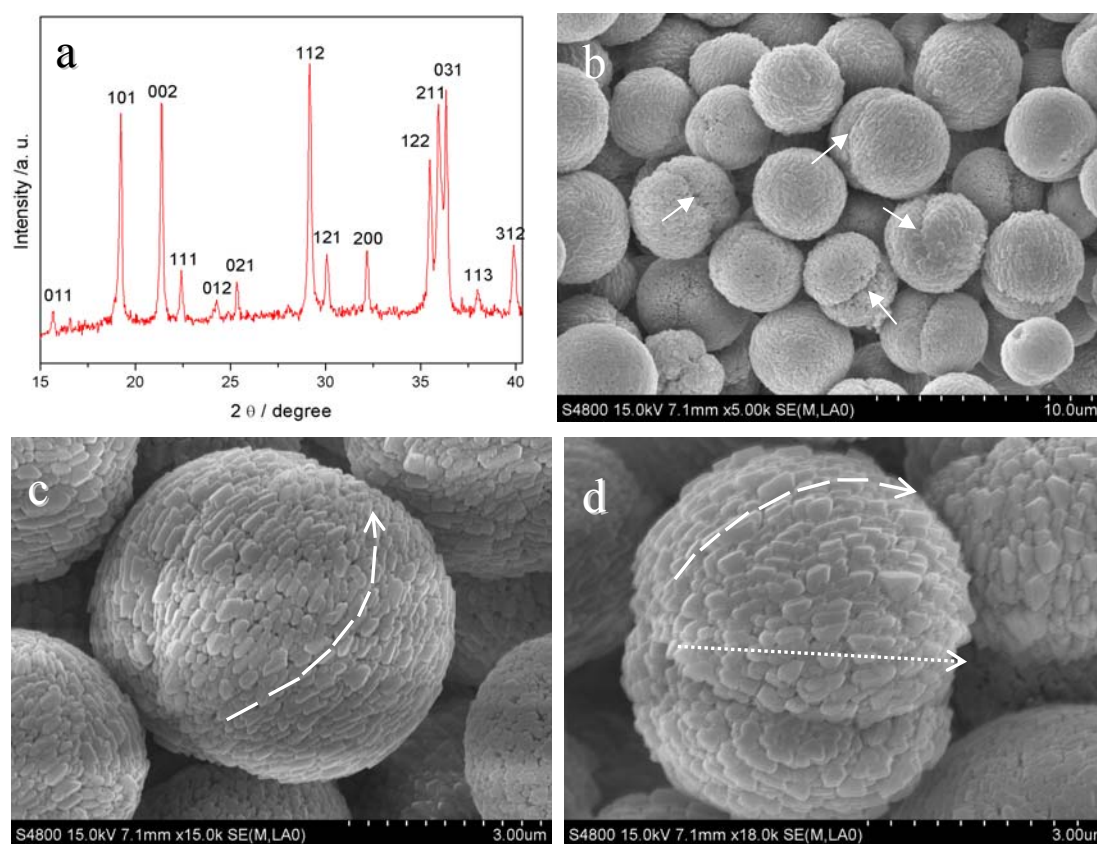
Fig. 1 (a) XRD pattern of the sample. (b) FESEM image of the sample. (c), (d) is the magnified
FESEM images of the sample.

The composition and phase structure of the sample was measured by the X-ray powder

diffractometer. All the diffraction peaks (Fig. 1a) could be well indexed to the monoclinic

structure of $Cu_2SO_3 \cdot CuSO_3 \cdot 2H_2O$ (JCPDS 19-0408), indicating the high purity and crystallinity of

the samples. FESEM image in Fig. 1b revealed that the products consisted of microspheres and

the average diameters of the microspheres were *ca.* 5 μm. The arrows marked in the image

indicated the microspheres were pseudospherical, comprising two hemispheres. The magnified SEM images (Fig. 1c and d) showed the detailed structure of microspheres, which were made of particles *ca.* 200-350 nm in size, but not be the random aggregate of particles. These particles arranged on the hemisphere surface in the crystallographically oriented fashion. The ordered arrangement fashion strongly suggested that the build units of microspheres were small particles, and their crystallization mechanism was a nonclassical crystallization process according to CÖlfen definition[34].
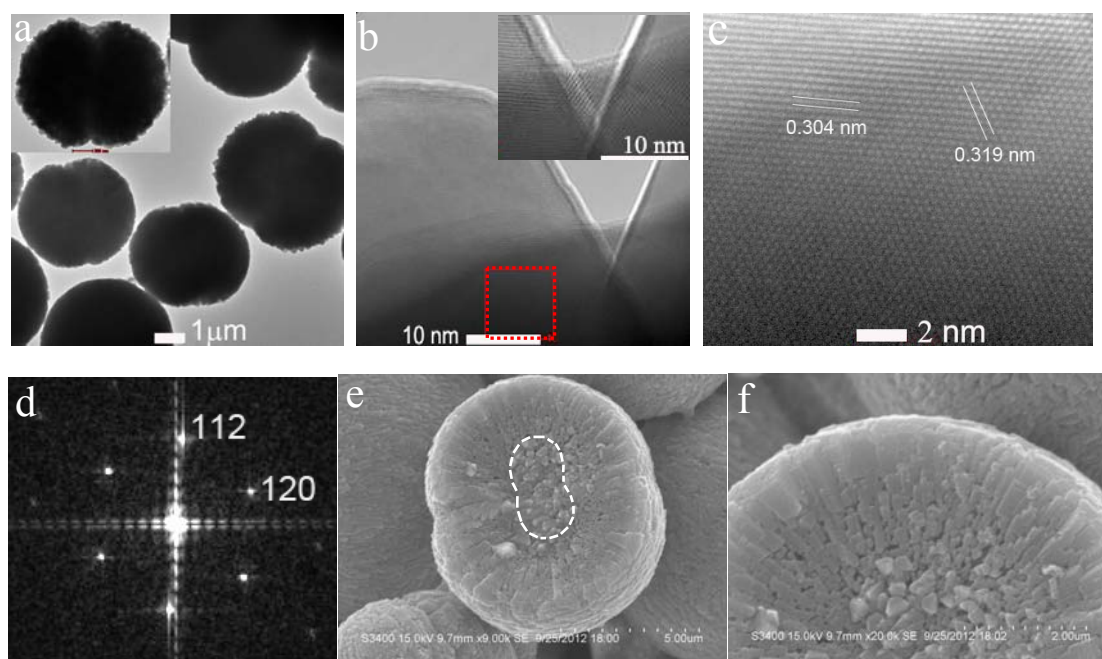
Fig. 2 (a) TEM image of $Cu_2SO_3 \cdot CuSO_3 \cdot 2H_2O$ mesocrystalline spheres (inset individual microsphere). (b) HRTEM image of microsphere edges (inset high magnification HRTEM image). (c) HRTEM image corresponding to a red rectangle area in Fig 2b. (d) Corresponding lattice fast-Fourier-transform pattern of Fig. 2c. (e) SEM image of one broken microsphere. (f) is the enlarged image of Fig. 2e.

The morphologies of the products were further examined by transmission electron microscope. The samples adopted an "8"-shaped structure and consisted of two hemispheres. TEM images (Fig. 2a and inset), in accord with the SEM images, showed the clear interface between the crystal halves. The edges of spheres consisted of well-aligned particles (Fig. 1c and d). The low magnification HRTEM images of adjacent particles (Fig. 2b) and their boundary (insetting in Fig. 2b) indicated clear continuous lattice fringes, which evidenced very single crystal structure of submicro-particles. Fig. 2c displayed that enlarged images originated from the marked

red area in the Fig. 2b showed the resolved lattice spacing of 0.304 and 0.319 nm, which corresponded to (112) and (120) planes of monoclinic phase respectively. Corresponding lattice Fourier-transform pattern (Fig. 2d) further corroborated $Cu_2SO_3 \cdot CuSO_3 \cdot 2H_2O$ crystalline nature by showing clear points consistent with XRD pattern. Fortunately SEM images of one broken microsphere (Fig. 2e and f) helped us observe their inner structure. The inner structure had two parts: a peanut-like core consisting of packed particles (area marked by white dashed line in Fig. 2e), and a shell composed of particles in oriented attachment fashion with radiated structure. Careful observation can find that the sizes of particles in the outer shell are larger than that of particles in the inner shell. The voids between the particles were apparently observed. These results fully indicated the typical character of the mesocrystal assembly.
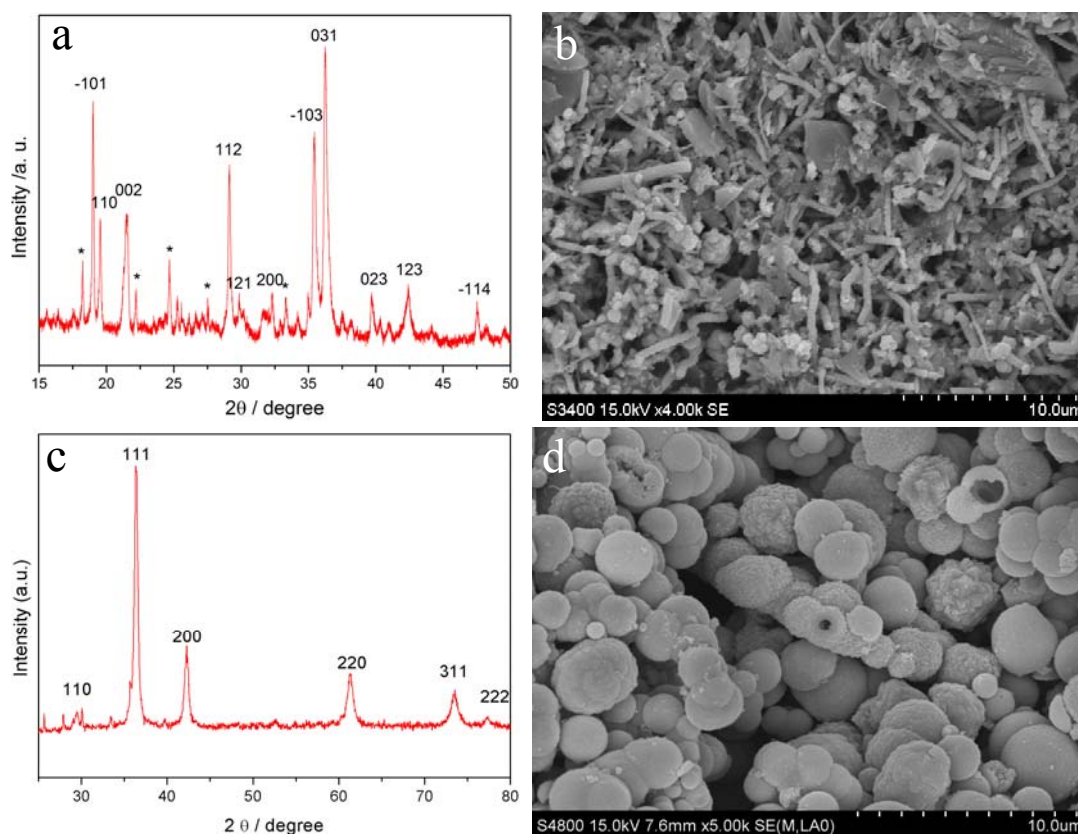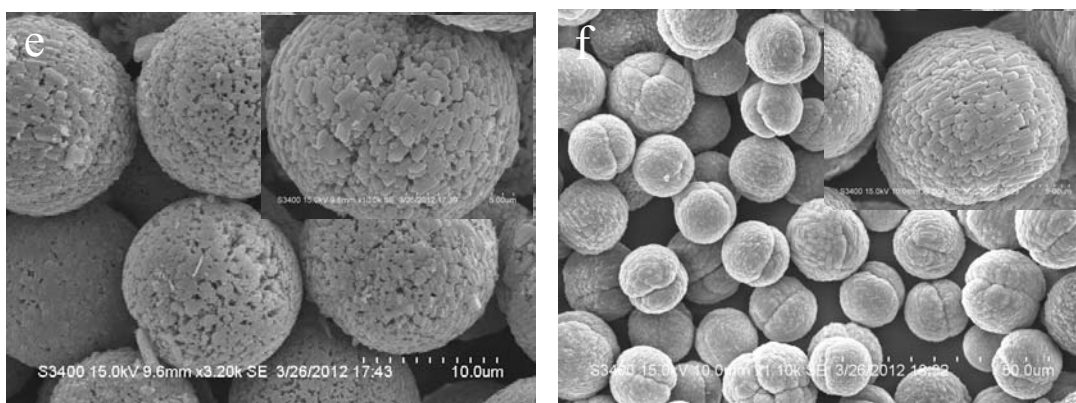
Fig. 3 (a) XRD pattern, (b) SEM image of the products obtained in the absence of acetic acid at ambient temperature. (c) XRD pattern, (d) SEM image of Cu$_2$O obtained in the absence of acetic acid at 90℃ for 5 h. SEM images of the samples obtained at the different reaction times: (e) 30 s, (f) 2 h respectively in the presence of concentration acetic acid.

In order to explore the formation mechanism of mesocrystalline spheres, controlled experiments were carried out. Without acetic aid, slurry immediately formed when CuAc$_2$ aqueous solution mixed with Na$_2$SO$_3$ aqueous solution at the ambient temperature. pH meter indicated pH value of the solution was *ca.* 5.4. The slurry was collected by centrifugation, water-washing and dry. XRD pattern in Fig. 3a showed that phases of the products included phase of monoclinic Cu$_3$(SO$_3$)$_3$·2H$_2$O (JCPDS 73-1606) and other unknown materials. SEM image (Fig. 3b) showed that the morphologies of the products included rods and micro-scale particles. When the slurry was heated to 90℃ in the oven and the temperature was kept for 5 h, the slurry transformed into red precipitate. XRD pattern in the Fig. 3c showed that it was Cu$_2$O with cubic phase (JCPDF 05-0667). SEM image (Fig. 3d) further showed the shape of the product was hollow sphere. As we known, Na$_2$SO$_3$ has reducibility and can reduce Cu^{2+} to obtain Cu$_2$O followed equation (1) below. But the experiments evidenced that the reaction could occur only when temperature was above 80℃. When using concentration acetic acid to regulate the pH value of the solution to *ca.* 4, the situation was quite different. The slurry became transparent in a short time and the reaction proceeded fast. Further experiments indicated that no red precipitates produced when pH valve was above 4.6. The reaction possibly proceeded according to equation 2 and 3. In low pH value (pH<4.6), SO$_3^{2-}$ can reduce Cu^{2+} to Cu$^+$ at low temperature, resulting in formation of Cu$_2$SO$_3$·CuSO$_3$·2H$_2$O [24, 27]. Time-dependant experiments were carried out. Filtration method was used to end reaction fast by solid-solution separation. Comparing the SEM images of the products obtained at 30 s (Fig. 3e), 15 min (Fig. 1b-d), and 2 h (Fig. 3f) respectively, the morphologies of

the products were almost same. It evidenced the formation rate of mesocrystalline microspheres was fast. The possible formation mechanism of mesocrystalline microspheres was as follows: At the beginning, fast produced crystals aggregated into peanut-like assembly as a nucleus for crystal further growing up. As the reaction proceeding, the reaction rate became slow and crystals newly born attached on the peanut-like nucleus in oriented attachment fashion until forming mesocrystals structure. At the early stage, the density of the particles in the initial structure was lower and large voids between particles were clearly observed (Fig. 3e); With the reaction proceeding, the concentration of the reaction species and therefore the reaction rate decreased, while the crystals attached on the nucleus grew up gradually and the gap between crystals reduced gradually (seeing Fig. 3f and 2f). Finally the mesocrystalline spheres composed of two semispheres were obtained due to the nucleus having a peanut-like shape. The details of the formation mechanism are not very clear at this moment. Thus further work is needed.

$$2Cu(Ac)_2 + 3Na_2SO_3 \rightarrow Cu_2O + Na_2SO_4 + 4NaAc + 2SO_2 \qquad (1)$$

$$SO_3^{2-} + H^+ = H_2SO_3 \qquad (2)$$

$$3Cu(Ac)_2 + 5H_2SO_3 + 2H_2O = [Cu_2SO_3 \cdot CuSO_3 \cdot 2H_2O] + 10H^+ + 2SO_4^{2-} + 6Ac^- + SO_2 \qquad (3)$$
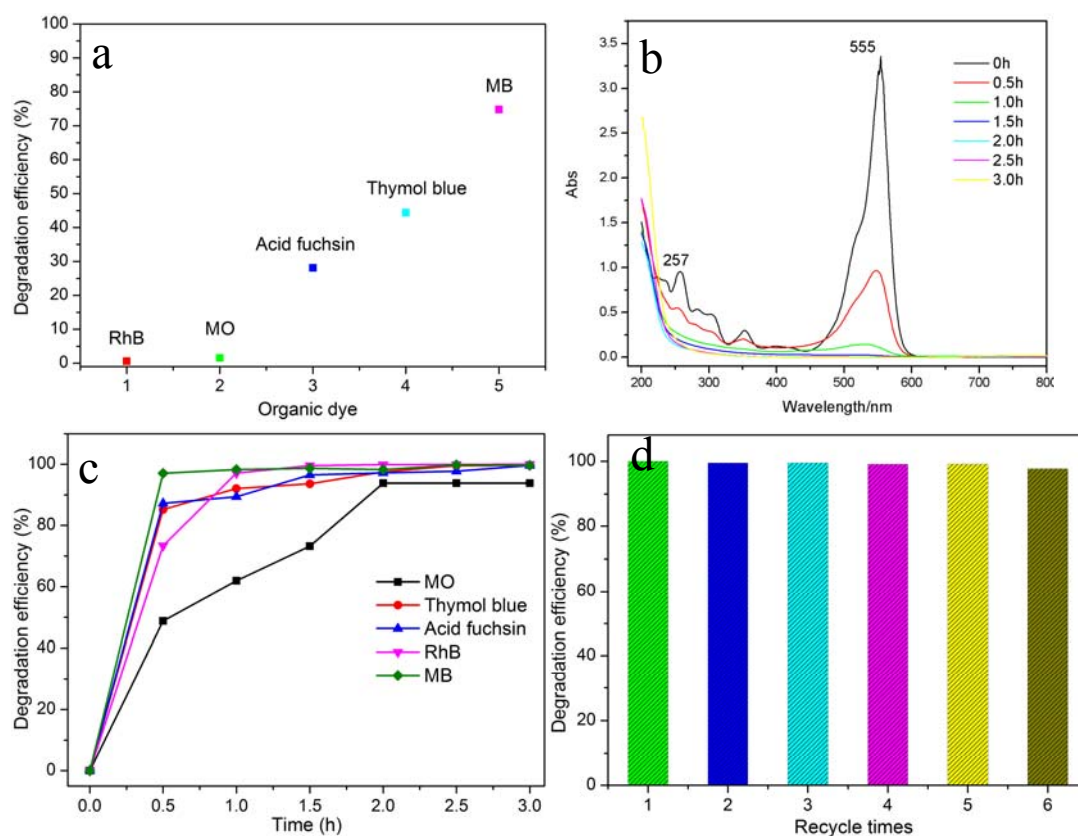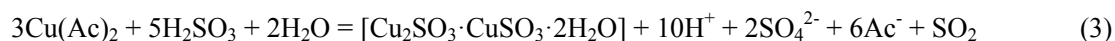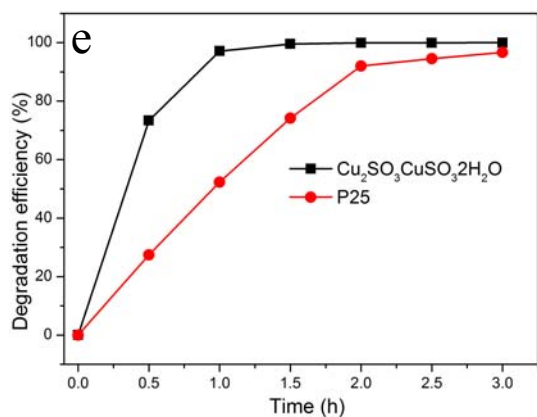
Fig. 4 (a) Photocatalytic degradation of different organic dyes: RhB, MO, acid fuchsin, thymol blue, MB without $Cu_2SO_3 \cdot CuSO_3 \cdot 2H_2O$ under UV light irradiation for 3 h. (b) Temporal UV-vis absorption spectral changes for the RhB solution over $Cu_2SO_3 \cdot CuSO_3 \cdot 2H_2O$ as a function of UV irradiation time from 0 to 3 h respectively. (c) Photocatalytic degradation curves of different organic dyes over $Cu_2SO_3 \cdot CuSO_3 \cdot 2H_2O$. (d) Photocatalytic degradation efficiency of RhB over $Cu_2SO_3 \cdot CuSO_3 \cdot 2H_2O$ versus recycle times. (e) Photocatalytic degradation curves of RhB (20 $mg \cdot L^{-1}$) over $Cu_2SO_3 \cdot CuSO_3 \cdot 2H_2O$ (0.6 $mg \cdot L^{-1}$) and P25 (0.6 $mg \cdot L^{-1}$) respectively.

In order to evaluate the photocatalytic activity of mesocrystalline $Cu_2SO_3 \cdot CuSO_3 \cdot 2H_2O$, aqueous solutions containing different organic dyes such as RhB, MB, MO, thymol blue, and acid fuchsin were irradiated on mesocrystalline microspheres under UV light irradiation. For comparison, the blank experiments without catalysts were carried out. Fig. 4a showed that RhB was not degraded, and the decomposition of MO was less than 1.5%, that of acid fuchsin, thymol blue and MB were 28%, 44% and 75% respectively after 3 h of irradiation. However, the results were quite different by using $Cu_2SO_3 \cdot CuSO_3 \cdot 2H_2O$ catalyst. Fig. 4b displayed the temporal evolution of the spectral changed during the photodegradation of RhB. The absorption band of RhB at 555 nm remarkably decreased with the reaction proceeding and the adsorption peak gradually shifted toward the blue region. The color of the dispersion solution changed from an initial red color to light green-yellow, and disappeared after 1.5 h of irradiation. The temporal evolution of the spectral changed during the photodegradation of MB, MO, thymol blue, and acid fuchsin were presented in supporting information (SI)-1. For MO, the degradation efficiency was less than 1.5% without catalysts, while in the photocatalytic decomposition, the degradation efficiency was up to 49% after 0.5 h (Fig. 4c) and 94% after 2 h. Although acid fuchsin, thymol blue and MB could be degraded to a certain extent under UV irradiation without the catalysts, they

could be completely decomposed after 3 h in the present of the catalysts. In addition, degradation efficiencies of acid fuchsin, thymol blue and MB were up to 85%, 87% and 97% respectively after 0.5 h of light irradiation (Fig. 4c). One can see that the decomposition rate of organic dyes on the catalysts was faster than that in the absence of the catalysts. The above results evidenced $Cu_2SO_3 \cdot CuSO_3 \cdot 2H_2O$ could accelerate decomposition of the organic dyes or completely degrade the organic dye molecules in the solution. To investigate the stability, $Cu_2SO_3 \cdot CuSO_3 \cdot 2H_2O$ was used repeatedly six times and the catalyst can be recovered easily by filtration method. As a typical example, the photocatalytic data of RhB was showed in Fig. 4d and the degradation efficiency reached 97.7% after six cycles. $Cu_2SO_3 \cdot CuSO_3 \cdot 2H_2O$ exhibited very stable photocatalytic activity. As a comparison, the RhB photodegraded on TiO_2 (P25) was also performed. The RhB concentrations versus reaction time for both the $Cu_2SO_3 \cdot CuSO_3 \cdot 2H_2O$ and P25 systems were plotted in Fig. 4e. Photocatalytic efficiencies for RhB on $Cu_2SO_3 \cdot CuSO_3 \cdot 2H_2O$ and P25 were 73% and 27% respectively for irradiating 0.5 h. RhB was completely photodegraded on $Cu_2SO_3 \cdot CuSO_3 \cdot 2H_2O$ in 1.5 h, while 25% RhB remained in the reaction by P25. Therefore, $Cu_2SO_3 \cdot CuSO_3 \cdot 2H_2O$ had better photocatalytic activity in RhB degradation reaction than P25. In addition, the diameter of P25 was *ca.* 21 nm. It was difficult to be handled after reaction, but $Cu_2SO_3 \cdot CuSO_3 \cdot 2H_2O$ microspheres can be easily separated from solution by using simple filtration or decantation method after sediment. All of these demonstrated that $Cu_2SO_3 \cdot CuSO_3 \cdot 2H_2O$ mesocrystalline spheres had not only excellent photocatalytic activity but also had good stability and easy post-treatment.
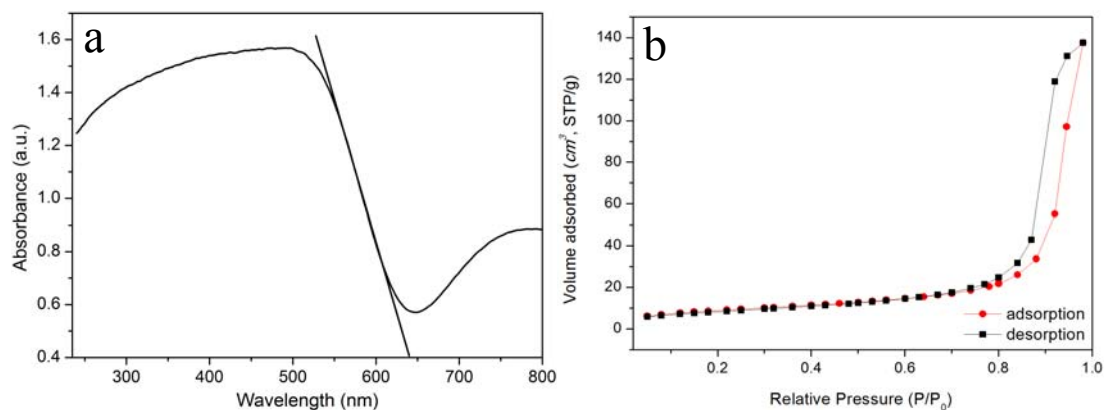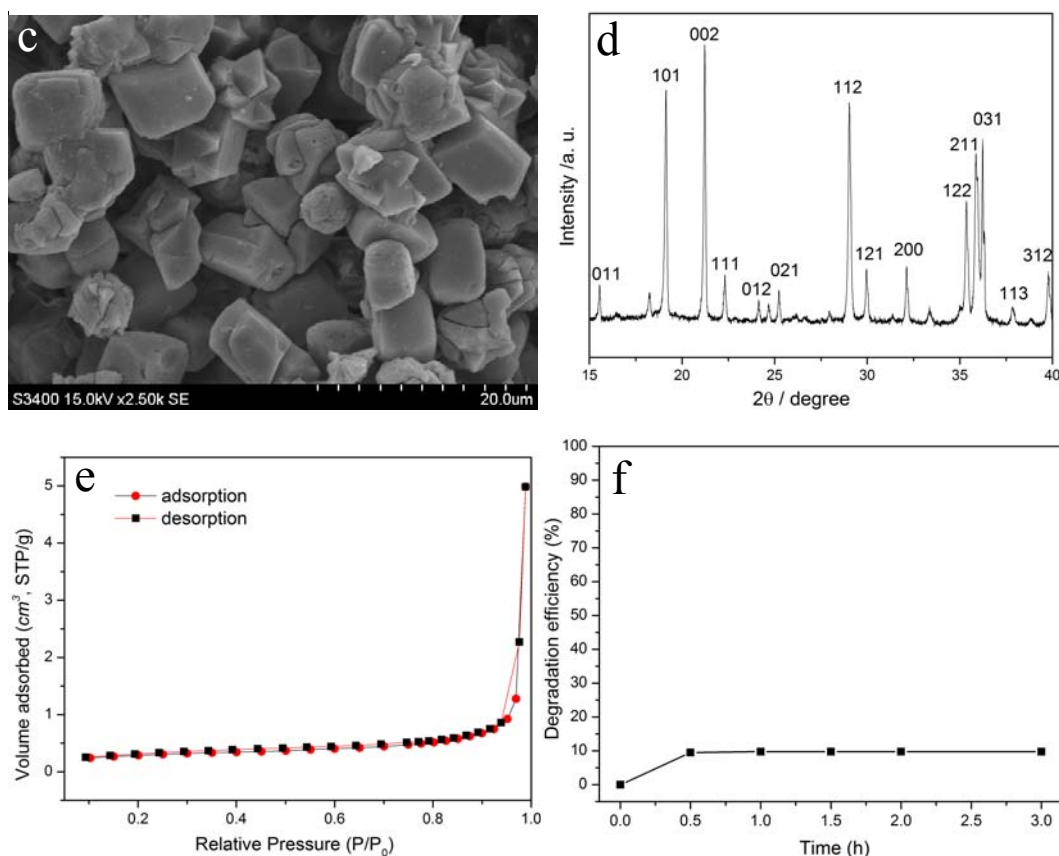
Fig. 5 (a) UV-vis diffuse reflectance spectra, (b) Nitrogen adsorption–desorption of the $Cu_2SO_3 \cdot CuSO_3 \cdot 2H_2O$ mesocrystalline microspheres. (c) SEM image, (d) XRD pattern, and (e) nitrogen adsorption–desorption of $Cu_2SO_3 \cdot CuSO_3 \cdot 2H_2O$ irregular particles. (f) Photocatalytic degradation curves of RhB (20 mg·L^{-1}) over irregular particles (0.6 mg·L^{-1}).

DRS is a useful tool for charactering light absorption and band gap in optical materials. Fig. 5a showed the broad absorption in the range of 250-550 nm. The absorption edge of $Cu_2SO_3 \cdot CuSO_3 \cdot 2H_2O$ mesocrystalline microspheres occured at about 640 nm, and the band gap energy was estimated to be *ca.* 1.94 eV. BET specific surface areas of $Cu_2SO_3 \cdot CuSO_3 \cdot 2H_2O$ mesocrystalline microspheres were investigated by using nitrogen adsorption-desorption measurement (Fig. 5b). The BET specific surface areas of the products calculated from the linear part of the BET plot is *ca.* 32 m^2·g^{-1}. The peak of the pore size distribution calculated by Barrett–Joyner–Halenda (BJH), derived from desorption data, was located at 17 nm (SI-2). The pore size calculated from the BJH result was attributed to the voids between the particles. In order to explore the factors of influencing the photocatalytic activity, the irregular shape of $Cu_2SO_3 \cdot CuSO_3 \cdot 2H_2O$ particles were synthesized (see detailed experimental procedure in the SI-3). SEM image of the product showed the range of sizes was *ca.* 5-8 μm. XRD pattern in Fig. 5d

12

could be well indexed to the monoclinic $Cu_2SO_3 \cdot CuSO_3 \cdot 2H_2O$ (JCPDS 19-0408). BET specific surface areas of the products (Fig. 5e) was *ca.*1.5 $m^2 \cdot g^{-1}$. Using irregular particles as photocatalysis, photocatalytic efficiencies for RhB were *ca* 10% after 3 h of irradiation (Fig. 5f). Compared with irregular particles, $Cu_2SO_3 \cdot CuSO_3 \cdot 2H_2O$ mesocrystalline microspheres have better photocatalytic activity in RhB degradation reaction.
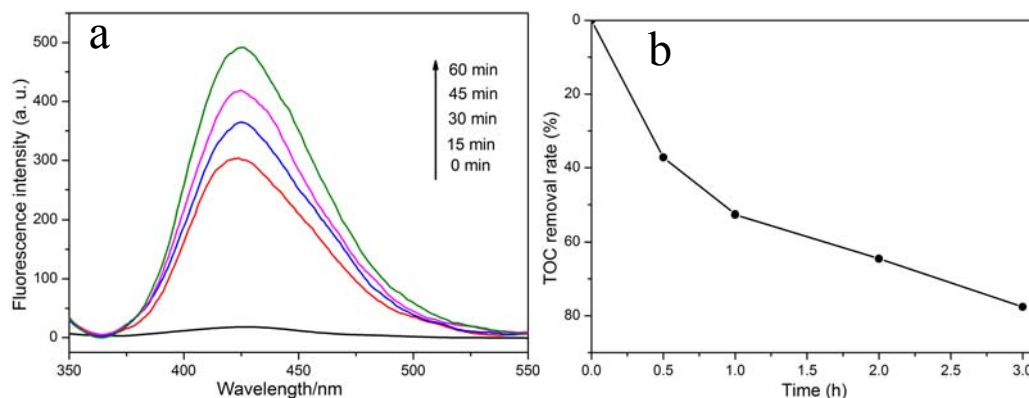
Fig. 6 (a) PL spectral changes observed during irradiation of the $Cu_2SO_3 \cdot CuSO_3 \cdot 2H_2O$ mesocrystalline microspheres prepared in a 1.5 $mmol \cdot L^{-1}$ basic solution of terephthalic acid (excitation at 315 nm). Each fluorescence spectrum was recorded every 15 min of UV illumination. (b) TOC removal plots of RhB over $Cu_2SO_3 \cdot CuSO_3 \cdot 2H_2O$ mesocrystalline microspheres under UV light irradiation.

Terephthalic acid readily reacted with •OH to produce highly fluorescent product, 2-hydroxyterephthalic acid. Photoluminescence (PL) technique with terephthalic acid as a probe molecule has been used to detect if hydroxyl radicals (•OH) produced on the water/photocatalysts interface [35, 36]. The PL emission spectra excited at 315 nm from terephthalic acid solution were measured every 15 min of illumination. Fig. 6a showed that PL intensity at about 425 nm gradually increased with the irradiation time prolonging. Additionally, there was almost no fluorescence signal in the blank test (no photocatalyst). This suggested that •OH was really produced on water/$Cu_2SO_3 \cdot CuSO_3 \cdot 2H_2O$ interface under ultraviolet light irradiation and the fluorescence was caused by chemical reactions of TA with •OH via photocatalytic reactions [37-41]. The above result evidenced that hydroxyl radicals were the main active species that could oxidize the adsorbed organic pollutants. In addition, the mineralization property of the $Cu_2SO_3 \cdot CuSO_3 \cdot 2H_2O$ photocatalysts was investigated. The TOC removal rates of RhB over $Cu_2SO_3 \cdot CuSO_3 \cdot 2H_2O$ mesocrystalline microspheres could reach 64.8% in 2 h of photocatalytic

reaction, with the irradiation time increasing, TOC removal rate of RhB in 3 h reached 77.6% (see Fig. 6b). This rate of TOC reduction of $Cu_2SO_3 \cdot CuSO_3 \cdot 2H_2O$ mesocrystalline microspheres was slower than that of the degradation of dye, which was nearly 100% discoloration for RhB in 2h shown Fig. 4c [42]. The decreasing TOC rate of $Cu_2SO_3 \cdot CuSO_3 \cdot 2H_2O$ mesocrystalline microspheres indicated that RhB was first ring cleavage and then converted into CO_2.

In addition, the possible reasons for the good photocatalytic activity of $Cu_2SO_3 \cdot CuSO_3 \cdot 2H_2O$ mesocrystalline microspheres are as following: First, porous character of mesocrystal will increase its specific surface area. Comparing with bulk material (less than several $m^2 \cdot g^{-1}$), the BET surface area of $Cu_2SO_3 \cdot CuSO_3 \cdot 2H_2O$ mesocrystalline spheres (*ca.* 32 $m^2 \cdot g^{-1}$) is several time increasing, which will improve the catalytic performance of the mesocrystalline spheres a lot. In addition, open pores could allow the penetration of light and diffusion of dyes solution into the photocatalyst, moreover, pores could increase the opportunity of the lights being absorbed via multiple reflection of light, therefore, increase its utilization [13, 43, 44]. Second, the small sizes of submicro-particles composed of mesocrystalline microspheres short the times of the electrons and holes reaching surface of submicro-particles and thus decrease the combination rate between electrons and holes which facilitates the degradation of pollutant [17]. Third, microscale $Cu_2SO_3 \cdot CuSO_3 \cdot 2H_2O$ mesocrystalline spheres are not easy to aggregate in the photocatalytic reaction process, which is important for post-treatment and recycle use with high photocatalytic activity.

4. Conclusion

In summary, we have synthesized $Cu_2SO_3 \cdot CuSO_3 \cdot 2H_2O$ mesocrystalline microspheres by a facile method. The formation mechanism was proposed. Acetic acid played a key role to prepare $Cu_2SO_3 \cdot CuSO_3 \cdot 2H_2O$ mesocrystalline microspheres. Mesocrystalline microspheres were composed of submicro-particles in oriented fashion. Under UV light irradiation, $Cu_2SO_3 \cdot CuSO_3 \cdot 2H_2O$ mesocrystalline spheres would catalyze decomposition of the organic dyes in solution. The big diameters of microspheres prevented from deactivation of the catalyst via further aggregation and made its post-treatment easy. $Cu_2SO_3 \cdot CuSO_3 \cdot 2H_2O$ mesocrystalline microspheres withstood high photocatalytic property after cycling several times. They have promising application for the treatment of the contaminated water. A series of works in the system

are underway.

Acknowledgements

References

1 A. Fujishima and K. Honda, *Nature,* 1972, **238,** 37-38.

2 C. C. Chen, W. H. Ma and J. C. Zhao, *Chem. Soc. Rev.,* 2010, **39,** 4206–4219.

3 D. Q. He, L. L. Wang, H. Y. Li, T. Y. Yan, D. J. Wang and T. F. Xie, *CrystEngComm.,* 2011, **13,** 4053–4059.

4 H. Tada, T. Kiyonaga and S. I. Naya, *Chem. Soc. Rev.,* 2009, **38,** 1849–1858.

5 C. S. Pan and Y. F. Zhu, *Environ. Sci. Technol.,* 2010, **44,** 5570–5574.

6 H. B. Fu, C. S. Pan, W. Q. Yao and Y. F. Zhu, *J. Phys. Chem. B.,* 2005, **109,** 22432-22439.

7 I. Ali, *Chem. Rev.,* 2012, **112,** 5073−5091.

8 C. Burda, X. B. Chen, R. Narayanan and M. A. El-Sayed, *Chem. Rev.,* 2005, **105,** 1025-1102.

9 S. Linic, P. Christopher and D. B. Ingram, *Nat. Mater.,* 2010, **10***,* 911-921.

10 J. X. Fang, B. J. Ding and H. Gleiterb, *Chem. Soc. Rev.,* 2011, **40,** 5347–5360.

11 R. Q. Song and H. CÖlfen, *Adv. Mater.,* 2010, **22,** 1301-1330.

12 M. J. McCall, *Nat. Nanotechnology.,* 2011, **6,** 613–614.

13 Z. Fang, L. Y. Long, S. H. Hao, Y. X. Song, T. T. Qiang and B. Y. Geng, *CrystEngComm,* 2014, **16,** 2061–2069.

14 M. S. Wang, Y. P. Zhang, Y. J. Zhou, F. W. Yang, E. J. Kim, S. H. Hahn and S. G. Seong, *CrystEngComm.,* 2013, **15,** 754–763.

15 Z. F. Bian, T. Tachikawa, P. Zhang, M. Fujitsuka and T. Majima, *J. Am. Chem. Soc.,* 2014, **136,** 458−465.

16 D. W. Hu, W. X. Zhang, Y. Tanaka, N. Kusunose, Y. G. Peng and Q. Feng, *Cryst. Growth Des.,* 2015, **15**, 1214−1225.

17 L. Zhou and P. O'Brien, *J. Phys. Chem. Lett.,* 2012, **3,** 620−628.

18 D. Zhang, G. Li, F. Wang and J. C. Yu, *CrystEngComm.,* 2010, **12,** 1759-1763.

19 B. Hu, L. H. Wu, S. J. Liu, H. B. Yao, H. Y. Shi, G. P. Li and S. H. Yu, *Chem. Commun.,* 2010, **46,** 2277-2279.

20 P. Tartaj, *Chem. Commun.,* 2011, **47,** 256-258.

21 L. Zhang, X. F. Cao, X. T. Chen and Z. L. Xue, *J. Colloid Interface Sci.,* 2011, **354,** 630-636.

22 K. X. Yao and H. C. Zeng, *J. Phys. Chem. C.,* 2009, **113,** 1373-1385.

23 L. Zhang, X. F. Cao, Y. L. Ma, X. T. Chen and Z. L. Xue, *New J. Chem.,* 2010, **34,** 2027-2033.

24 M. E. Chevreul, *Ann. Chim.*, 1812, **83,** 181.

25 P. Kierkgaard and B. Nyberg, *Acta Chem. Scand.,* 1965, **19,** 2189-2199.

26 M. H. Conkllnt and M. R. Hoffmann, *Environ. Sci. Technol.,* 1988, **22,** 883-891.

27 M. H. Conkllnt and M. R. Hoffmann, *Environ. Sci. Technol.,* 1988, **22,** 891-898.

28 D. Wang and A. D.Tang, *Adv. Mater. Res.,* 2012, **538-541,** 2405-2408.

29 L. A. Silva and J. B. Andrade, *J. Chem. Edu.,* 2010, **87,** 530-532.

30 L. A. Silva, J. R. Matos and J. B. Andrade, *Thermochim. Acta.,* 2000, **360,** 17-27.

31 M. Inoue, H. Grijalva, M. B. Inoue and Q. Fernando, *Inorg. Chim. Acta.,* 1999, **295,** 125–127.

32 T. Calban, S. Kusiu and S. Colak, *Chem. Eng. Comm.,* 2009, **196,** 1018–1029.

33 L. A. Silva, J. R. Matos and *J. B.* Andrade, *J. Braz. Chem. Soc.,* 2004, **15,** 170-177.

34 H. Cölfen, M. Antonietti, *Angew. Chem. Int. Ed.,* 2005, **44,** 5576-5591.

35 J. G. Yu, W. G. Wang, B. Cheng and B. L. Su, *J. Phys. Chem. C*, 2009, **113,** 6743–6750.

36 Y. Sang, L. Kuai, C. Y. Chen, Z. Fang and B. Y. Geng, *ACS Appl. Mater. Interfaces.,* 2014, **6,** 5061−5068.

37 J. X. Wang, H. Ruan, W. J. Li, D. Z. Li, Y. Hu, J. Chen, Y. Shao and Y. Zheng, *J. Phys. Chem. C,* 2012, **116,** 13935−13943.

38 K. Ishibashi, A. Fujishima, T. Watanabe and K. Hashimoto, *Electrochem. Commun.,* 2000, **2,** 207-210.

39 M. J. Zhou, X. H. Gao, Y. Hu, J. F. Chen and X. Hu, *Appl. Catal. B: Environ.,* 2013, **138-139,** 1-8.

40 S. L. Wang, H. H. Qian, Y. Hu, W. Dai, Y. J. Zhong, J. F. Chen and X. Hu, *Dalton Trans.,* 2013, **42,** 1122–1128.

41 Y. Hu, X. H. Gao, L. Yu, Y. R. Wang, J. Q. Ning, S. J. Xu and X. W. Lou, *Angew. Chem. Int. Ed.,* 2013, **52,** 5636–5639.

42. C. S. Pan and Y. F. Zhou, *Environ. Sci. Technol.,* 2010, **44,** 5570–5574.

43 C. S. Pan and Y. F. Zhu, *J. Mater. Chem.,* 2011, **21,** 4235–4241.

44 J. X. Sun, G. Chen, J. Pei, R. C. Jin, Q. Wang and X. Y. Guang, *J. Mater. Chem.,* 2012, **22,** 5609–5614.

CrystEngComm Accepted Manuscript

The table of contents entry

Facile preparation of Chevreul's salt (Cu$_2$SO$_3$·CuSO$_3$·2H$_2$O) mesocrystalline microspheres and its high photocatalytic activity

Mingyun Guan*, Yan Jian, Jianhua Sun, Tongming Shang , Qi Liu, and Zheng Xu*
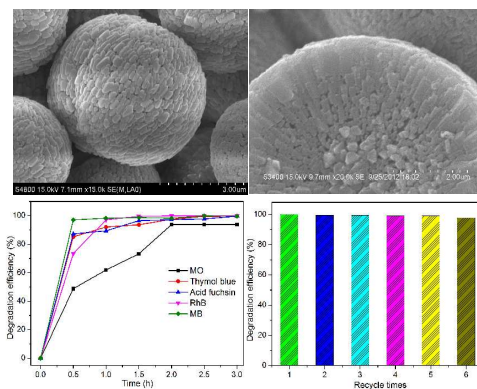
Cu$_2$SO$_3$·CuSO$_3$·2H$_2$O mesocrystalline microspheres with excellent photocatalytic performance, composed of submicro-particles in oriented fashion, are synthesized by a facile method.